Electronic structure and optical properties of quantum rods with wurtzite structure

Xin-Zheng Li and Jian-Bai Xia
Chinese Center of Advanced Science and Technology (World Laboratory), P.O.Box 8730, Beijing 100080, China
and Institute of Semiconductors, Chinese Academy of Sciences, P. O. Box 912, Beijing 100083, People's Republic of China
(Received 8 April 2002; published 20 September 2002)

The Hamiltonian of the wurtzite quantum rods with an ellipsoidal boundary is given after a coordinate transformation. The energies, wave functions, and transition possibilities are obtained as functions of the aspect ratio e with the same method we used on spherical dots. With an overall consideration of both the transition matrix element and the Boltzmann distribution we explained why the polarization factor increases with increasing e and approaches a saturation value, which tallies quite well with the experimental result. When e increases more and more S_z states are mixed into the ground, second, and third states of $J_z=1/2$, resulting in an increase of the emission of z polarization. It is just the linear terms of the momentum operator in the hole Hamiltonian that cause the mixing of S and P states in the hole ground state. The effects of the crystal field splitting energy, temperature, and transverse radius to the polarization are also considered. We also calculated the band gap variation with the size and shape of the quantum rods.

DOI: 10.1103/PhysRevB.66.115316 PACS number(s): 73.61.Ga, 78.66.Hf

I. INTRODUCTION

Compared with the quantum dots produced by molecular beam epitaxy (MBE), colloidal dots can be made by more simple procedures and with a highly monodisperse size range.[1–3] The band gap and oscillator strength can be tuned by changing the diameter of colloidal dots as can the optical properties.[4] If we do not just make spherical colloidal dots and produce ellipsoidal rods, there would more freedom with the tuning of these properties. Linearly polarized emission of slightly elongated quantum dots (quantum rods) has been reported with an experiment and a theoretical explanation of empirical pseudopotential calculations recently.[5] This discovery gives colloidal quantum dots a much more promising future because linearly polarized emissions have a much wider range of applications, such as biological labeling[6,7] and optoelectronic devices.[8] The method of artificially arranging materials this way has also been reported,[5] which makes us more confident of their future.

In this paper, we take the elongated colloidal quantum dots of CdSe with wurtzite structure as ellipsoidal cases. With a transformation of coordinates, we can get a Hamiltonian much like that of the spherical case, which has been studied systemically before.[9–11] This model is given in Sec. II. After obtaining the energies and wave functions, we found that the higher hole states consist of two different angular momentum components along the z axis, the first with 1/2, while the second with 3/2. We can get the energies and wave functions of the electron states with the same method. Because the lowest electron state is always the S state, we can see from the envelope function of these two kinds of hole states that only the $J_z=1/2$ states contribute to the emission with polarization along the z axis. We calculated the transition matrix elements from the first electron state to the two kinds of low-lying hole states and consider the Boltzmann distribution of the hole on the hole states. Then we combined these factors, and obtained the actual transition probability for polarization along each axis. The effects of the crystal-field splitting energy, temperature, and the radius of the rods on the polarization are considered. We also calculated the energy gap of the quantum rods with different shapes and sizes. These discussions and results are given in Sec. III. Finally, we draw a brief conclusion in Sec. IV.

II. MODEL AND CALCULATION

The hole Hamiltonian for wurtzite semiconductors such as CdS, CdSe, and ZnS was given in Ref. 9 by the following way. The total Hamiltonian is the summation of the Hamiltonian with zero spin-orbital coupling (SOC) and the spin-orbital coupling Hamiltonian. If we take the basic functions as $|1,1\rangle=(1/\sqrt{2})(X+iY)$, $|1,0\rangle=Z$, and $|1,-1\rangle=(1/\sqrt{2})\times(X-iY)$, the Hamiltonian of zero spin-orbital coupling can be written as

$$H_0=\frac{1}{2m_0}\begin{vmatrix} P_1 & S & T \\ S^* & P_3 & S \\ T^* & S^* & P_1 \end{vmatrix}, \tag{1}$$

where

$$\begin{aligned} P_1&=\gamma_1 p^2-\sqrt{\frac{2}{3}}\gamma_2 P_0^{(2)}, \\ P_3&=\gamma_1' p^2+2\sqrt{\frac{2}{3}}\gamma_2' P_0^{(2)}+2m_0\Delta_c, \\ T&=\eta P_{-2}^{(2)}+\delta P_2^{(2)}, \\ T^*&=\eta P_2^{(2)}+\delta P_{-2}^{(2)}, \\ S&=Ap_0 P_{-1}^{(1)}+\sqrt{2}\gamma_3' P_{-1}^{(2)}, \\ S^*&=-Ap_0 P_1^{(1)}-\sqrt{2}\gamma_3' P_1^{(2)}, \end{aligned} \tag{2}$$

where $P^{(2)}$ and $P^{(1)}$ are the second-order and first-order tensors of the momentum operator, respectively, and $p_0=\sqrt{2m_0\Delta_c}$. The effective-mass parameter for the CdSe we used is also given in Table I. The spin-orbital coupling Hamiltonian is written as

TABLE I. Parameters for CdSe in the actual calculation.

m_x	m_z	γ_1	γ_2	γ_2'	γ	γ_1'	γ_3'	A	Δ_c (meV)	λ (meV)
0.1756	0.1728	1.7985	0.7135	0.7970	1.4492	2.166	0.3779	1.7985	25	−139.3

$$H_{so}=\begin{vmatrix} -\lambda & 0 & 0 & 0 & 0 & 0 \\ 0 & 0 & 0 & \sqrt{2}\lambda & 0 & 0 \\ 0 & 0 & \lambda & 0 & -\sqrt{2}\lambda & 0 \\ 0 & \sqrt{2}\lambda & 0 & \lambda & 0 & 0 \\ 0 & 0 & -\sqrt{2}\lambda & 0 & 0 & 0 \\ 0 & 0 & 0 & 0 & 0 & -\lambda \end{vmatrix}. \tag{3}$$

Here we take $|11\rangle\uparrow=(1/\sqrt{2})(X+iY)\uparrow$, $|10>\uparrow=Z\uparrow$, $|1-1>\uparrow=1/\sqrt{2}(X-iY)\uparrow$, $|11\rangle\downarrow=(1/\sqrt{2})(X+iY)\downarrow$, $|10\rangle\downarrow=Z\downarrow$, and $|1-1\rangle\downarrow=(1/\sqrt{2})(X-iY)\downarrow$ as basic functions; X,Y, and Z are explained in Ref. 9 and the parameter we used for CdSe is given in Table I.

For our cases of quantum rods, the boundary condition is different from that of spherical quantum dots. In order to simplify our boundary condition into that of the spherical case, which has a better symmetrical characteristic,[12] we introduce a coordinate transformation that can change the boundary into the spherical one in the new coordinate system. The transformation is $x'=x$, $y'=y$, $z'=z/e$, where e is the aspect ratio of the ellipsoid, (x,y,z) is the actual coordinate and (x',y',z') is the transformed one. The hole Hamiltonian in the new coordinate changes as follows:

$$P_1=\left[\frac{(\gamma_1+\gamma_2)(1+2e^2)}{3e^2}-\frac{1}{e^2}\gamma_2\right]p^2 - \sqrt{\frac{2}{3}}\left[\frac{1}{e^2}\gamma_2-\frac{(1-e^2)(\gamma_1+\gamma_2)}{3e^2}\right]P_0^{(2)},$$

$$P_3=\left[\frac{(\gamma_1'-2\gamma_2')(1+2e^2)}{3e^2}+2\gamma_2'\frac{1}{e^2}\right]p^2 + 2\sqrt{\frac{2}{3}}\left[\gamma_2'\frac{1}{e^2}+\frac{(1-e^2)(\gamma_1'-2\gamma_2')}{6e^2}\right]P_0^{(2)}+2m_0\Delta_c,$$

$$S=Ap_0P_{-1}^{(1)}+\sqrt{2}\left(\gamma_3'\frac{1}{e}\right)P_{-1}^{(2)}, \tag{4}$$

$$S^*=-Ap_0P_1^{(1)}-\sqrt{2}\left(\gamma_3'\frac{1}{e}\right)P_1^{(2)},$$

$$T=\eta P_{-2}^{(2)}+\delta P_2^{(2)},$$

$$T^*=\eta P_2^{(2)}+\delta P_{-2}^{(2)}.$$

H_{so} does not change forms. After assuming that the electrons and holes are in infinite deep potential wells in the new coordinate system, we can calculate the energies and wave functions of the quantum rods. For the state of a specific z component of the total angular momentum $M=m+1/2$, the envelope function in the new coordinate can be expressed as follows:

$$\psi_{m+\frac{1}{2}}=\sum_{l,n}\begin{pmatrix} a_{ln}A_{ln}j_l(K_n^lr)Y_{l,m-1} \\ b_{ln}A_{ln}j_l(K_n^lr)Y_{l,m} \\ c_{ln}A_{ln}j_l(K_n^lr)Y_{l,m+1} \\ d_{ln}A_{ln}j_l(K_n^lr)Y_{l,m} \\ f_{ln}A_{ln}j_l(K_n^lr)Y_{l,m+1} \\ g_{ln}A_{ln}j_l(K_n^lr)Y_{l,m+2} \end{pmatrix}. \tag{5}$$

We expand the radial part of the envelope function with spherical Bessel functions of this form because these functions can express the same symmetrical characteristic of the boundary condition. Because we assume that the well is an infinitely deep one, the radial part is always zero on the edge. $\alpha_n^l=K_n^lR$ is the zero point of the l-order spherical Bessel function. The effective-mass Hamiltonian of the electron also changes into the new form:

$$H_e=\frac{p^2}{2m_a}-\frac{1}{2m_b}\sqrt{\frac{2}{3}}P_0^{(2)}, \tag{6}$$

where

$$\frac{1}{m_a}=\frac{1}{3}\left(\frac{2}{m_x}+\frac{1}{e^2m_z}\right),$$

$$\frac{1}{m_b}=\frac{1}{3}\left(\frac{1}{m_x}-\frac{1}{e^2m_z}\right). \tag{7}$$

III. RESULTS AND DISCUSSIONS

A. Electronic states

The effective mass parameters for CdSe used in this paper are given in Table I.[9] For the other parameters we use the transverse radius $R=2.1$ nm and the temperature $T=300$ K in order to compare our theoretical results with the experimental results.[5] We calculated the electron energy levels as functions of the aspect ratio e using the Hamiltonian (6). Because for CdSe, $m_x\approx m_z$ (see Table I), the electronic states are nearly isotropic at $e=1$. When $e>1$, only the component of the angular momentum along the z direction is the good quantum number. The second-order tensor of the momentum operator in Hamilronian (6) $P_0^{(2)}$ couples the l state with $l+2,l+4,\ldots$ states, so we expand the electron wave function as

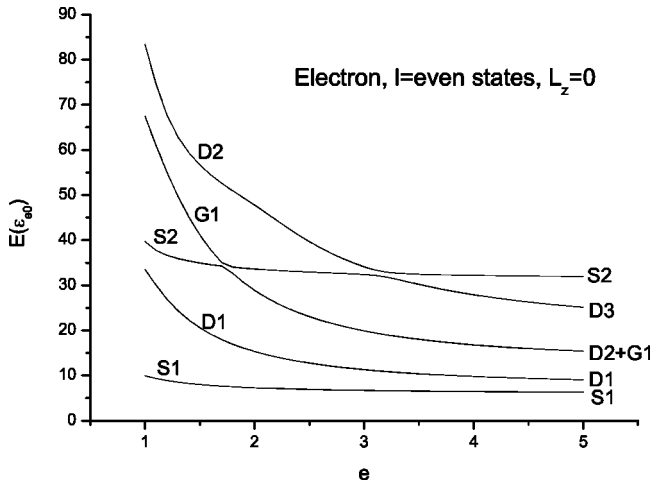

FIG. 1. Energies of electronic states of $L_z=0$ composed of even l states with respect to the bottom of the conduction band of quantum ellipsoids as functions of the aspect ratio e, in units of $\varepsilon_{e0}=(1/2m_x)[(\hbar/R)^2]$.

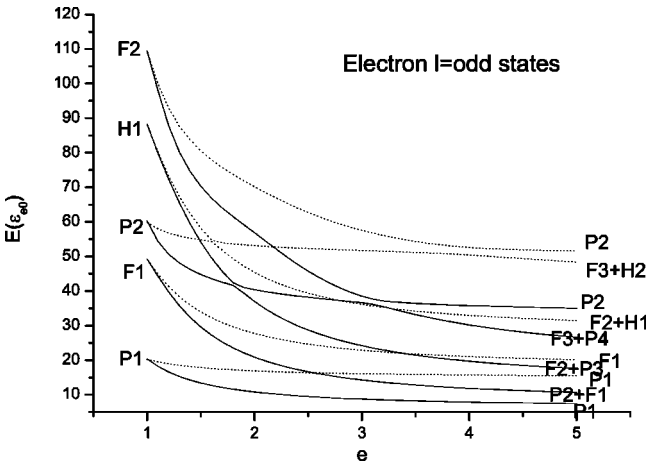

FIG. 2. Energies of $L_z=0$ and 1 composed of odd l states with respect to the bottom of the conduction band of quantum ellipsoids as a function of e, in units of ε_{e0}. The $L_z=0$ states are represented by solid curves while the $L_z=1$ are represented by dot curves.

$$\psi_{em}=\sum_{l,n} e_{ln}A_{ln}j_l(K_n^l r)Y_{l,m}. \tag{8}$$

Figure 1 shows the electron energy levels as functions of e for the l=even states with $L_z=0$ in units of $\varepsilon_{e0}=(1/2m_x)(\hbar/R)^2$. The signals S,D,G represent the main component in the wave function (8). From Fig. 1 we see that the energies of D and G states decrease with increasing e, but those of the S states change a little. It is because the wave function of the S state is independent of the z coordinate, so it is not affected when e increases. But the wave functions of the D and G states, Y_{20} and Y_{40}, are dependent of z, and their energies decrease when e increases.

Figure 2 shows the energies of the l=odd states as functions of e for $L_z=0$ and 1. At $e=1$, the energies of $L_z=0$ and $L_z=1$ states are degenarate due to the spherical symmetry. When $e>1$, the degeneracy is shifted, and the energies decrease with increasing e. The energies of the $L_Z=0$ states are always lower than those of the $L_z=1$ states; it can also be explained by the spherical harmonic functions Y_{10},Y_{11}, and Y_{30},Y_{31}, etc.

The wave function (8) consists of basic functions of different angular momentum $l,l+2,l+4,\ldots$. The larger the e, the stronger the mixing of different l basic functions.

B. Hole states

For CdSe the spin-orbital splitting energy of the valence band is larger compared to the confined energies of the hole states ($\Delta_{so}=0.4$ eV), so we have to consider the effect of the spin-orbital coupling, and use the Hamiltonian (3). In the case of ellipsoids, only the z component of the total angular momentum ($J=L+S, S=3/2$) is the good quantum number. The wave functions of the hole $J_z=1/2$ and 3/2 are written as [see Eq. (5)]

$$\psi_{1/2}=\sum_n \begin{pmatrix} a_{2n}|2-1\rangle_n+a_{4n}|4-1\rangle_n \\ b_{0n}|00\rangle_n+b_{2n}|20\rangle_n+b_{4n}|40\rangle_n \\ c_{2n}|21\rangle_n+c_{4n}|41\rangle_n \\ d_{1n}|1-1\rangle_n+d_{3n}|3-1\rangle_n+d_{5n}|5-1\rangle_n \\ f_{1n}|10\rangle_n+f_{3n}|30\rangle_n+f_{5n}|50\rangle_n \\ g_{1n}|11\rangle_n+g_{3n}|31\rangle_n+g_{5n}|51\rangle_n \end{pmatrix}\uparrow+\sum_n \begin{pmatrix} a'_{0n}|00\rangle_n+a'_{2n}|20\rangle_n+a'_{4n}|40\rangle_n \\ b'_{2n}|21\rangle_n+b'_{4n}|41\rangle_n \\ c'_{2n}|22\rangle_n+c'_{4n}|42\rangle_n \\ d'_{1n}|10\rangle_n+d'_{3n}|30\rangle_n+d'_{5n}|50\rangle_n \\ f'_{1n}|11\rangle_n+f'_{3n}|31\rangle_n+f'_{5n}|51\rangle_n \\ g'_{3n}|32\rangle_n+g'_{5n}|52\rangle_n \end{pmatrix}\downarrow \tag{9}$$

and

$$\psi_{3/2}=\sum_n \begin{pmatrix} a_{0n}|00\rangle_n+a_{2n}|20\rangle_n+a_{4n}|40\rangle_n \\ b_{2n}|21\rangle_n+b_{4n}|41\rangle_n \\ c_{2n}|22\rangle_n+c_{4n}|42\rangle_n \\ d_{1n}|10\rangle_n+d_{3n}|30\rangle_n+d_{5n}|50\rangle_n \\ f_{1n}|11\rangle_n+f_{3n}|31\rangle_n+f_{5n}|51\rangle_n \\ g_{3n}|32\rangle_n+g_{5n}|52\rangle_n \end{pmatrix}\uparrow+\sum_n \begin{pmatrix} a'_{2n}|21\rangle_n+a'_{4n}|41\rangle_n \\ b'_{2n}|22\rangle_n+b'_{4n}|42\rangle_n \\ c'_{4n}|43\rangle_n \\ d'_{1n}|11\rangle_n+d'_{3n}|31\rangle_n+d'_{5n}|51\rangle_n \\ f'_{3n}|32\rangle_n+f'_{5n}|52\rangle_n \\ g'_{3n}|33\rangle_n+g'_{5n}|53\rangle_n \end{pmatrix}\downarrow, \tag{10}$$

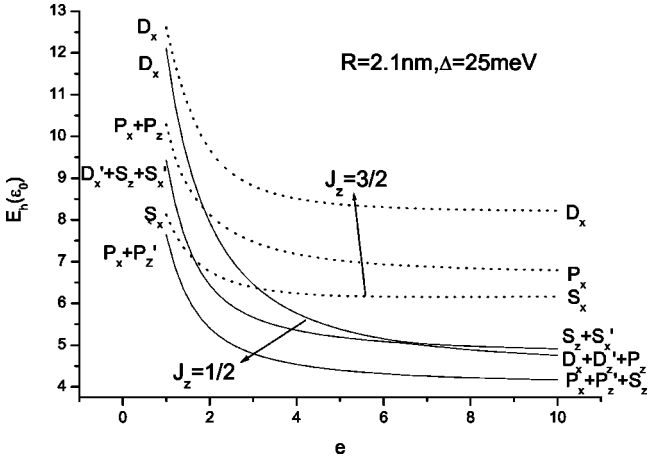

FIG. 3. Energies of the three highest hole states of $J_z=1/2$ and 3/2 with respect to the top of the valence band of quantum ellipsoids as functions of the aspect ratio e, in units of $\varepsilon_0=(\gamma_1/2m_0)\times[(\hbar/R)^2]$; the states for $J_z=3/2$ are represented by dot curves.

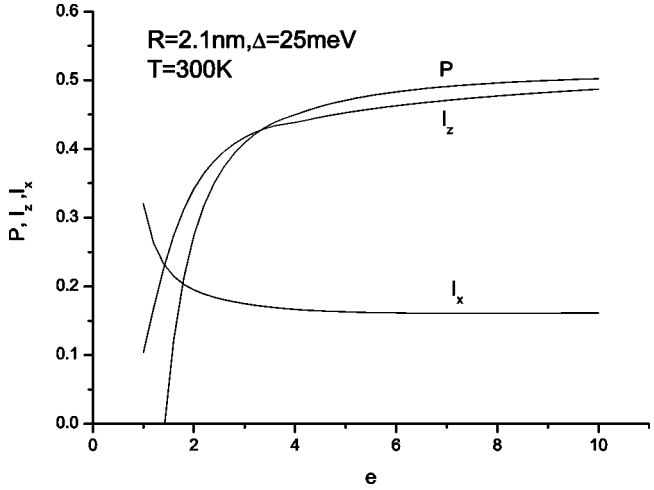

FIG. 4. The polarization factors P, optical transition strengths for two polarization I_z and I_x as a function of e for $T=300$ K, $\Delta_c=25$ meV, and $R=2.1$ nm.

respectively, where $|lm\rangle_n=A_{lm}j_l(K_n^l r)Y_{l,m}(\theta,\varphi)$ and the expansion is terminated at $l=5$.

Figure 3 shows the energies of three highest hole states of $J_z=1/2$ and 3/2 as functions of e, where the energies are calculated from the top of the valence band downwards. The signal of each curve represents the main components of its wave function (9) or (10). For example, for the state of $J_z=1/2$,S_z means that the main component is the $b_{0n}|00\rangle_n$ with the basic function $Z\uparrow$,S_x' means that the main component is the $a_{0n}'|00\rangle_n$ with the basic function $(1/\sqrt{2})(X+iY)\downarrow$, etc.

From Fig. 3 we see that the energies of $J_z=1/2$ states decrease with e faster than those of $J_z=3/2$ states. At $e=1$ the ground state of $J_z=1/2$ is the P_x state, and the ground state of $J_z=3/2$ is the S_x state, which is higher than that of $J_z=1/2$, so there will be a dark exciton in this case of $R=2.1$ nm, as shown in Ref. 9. For states of $J_z=1/2$, as e increases, the second state consists of more and more S_z component. When e equals nearly 6, the second and third states cross over, and at $e=10$ the third state is mainly the S_z state. Mainwhile, the ground state consists also of some S_z state added to the P_x state due to the linear terms of the momentum operator in the hole Hamiltonian [see Eqs. (1) and (2)], which cause the mixing of the S and P states in the hole ground state. On the other hand, the ground state of $J_z=3/2$ is always S_x state for $e=1$–10. It is just the increase of the S_z component in the ground, second, and third states of $J_z=1/2$ that causes the polarization along the z direction of luminescence in quantum ellipsoids of large aspect ratio.

C. Polarization of optical transition

Because the effective mass of the electron is much smaller than that of the hole, the spacing of energy levels of the electron is larger than that of the hole, so we only consider the optical transition from the electron ground state $S1$ to hole states. The wave function of the electron ground state is written as

$$\psi_e=\sum_n (e_{0n}|00\rangle_n+e_{2n}|20\rangle_n+e_{4n}|40\rangle_n)\uparrow \text{ or } \downarrow. \quad (11)$$

The optical transition probability is proportional to

$$|\langle\psi_e|\psi_{1/2}\rangle|^2=\begin{cases}\left[\sum_n (e_{0n}b_{0n}+e_{2n}b_{2n}+e_{4n}b_{4n})\right]^2, \\ \quad z \text{ polarization} \\ \frac{1}{2}\left[\sum_n (e_{0n}a_{0n}'+e_{2n}a_{2n}'+e_{4n}a_{4n}')\right]^2, \\ \quad x \text{ polarization}\end{cases} \quad (12)$$

and

$$|\langle\psi_e|\psi_{3/2}\rangle|^2=\frac{1}{2}\left[\sum_n (e_{0n}a_{0n}+e_{2n}a_{2n}+e_{4n}a_{4n})\right]^2, \quad x \text{ polarization}. \quad (13)$$

Multiply the Boltzmann distribution factor of each state, and sum up all contributions to the transitions of z and x polarizations. We then obtain the strengths of optical transition for two polarizations: I_z and I_x. Then the polarization factor is

$$P=\frac{I_z-I_x}{I_z+I_x}. \quad (14)$$

Figure 4 shows P, I_z, and I_x as functions of e, assuming that the temperature $T=300$ K. From Fig. 4 we see that P increases rapidly as e increases from 1 to 3; when e increases continuously, P approaches a saturation value about 0.5. This result is in good agreement with the experimental result,[5] except that the saturation value is smaller slightly than the experimental value 0.6. In the following we consider some factors affecting the polarization.

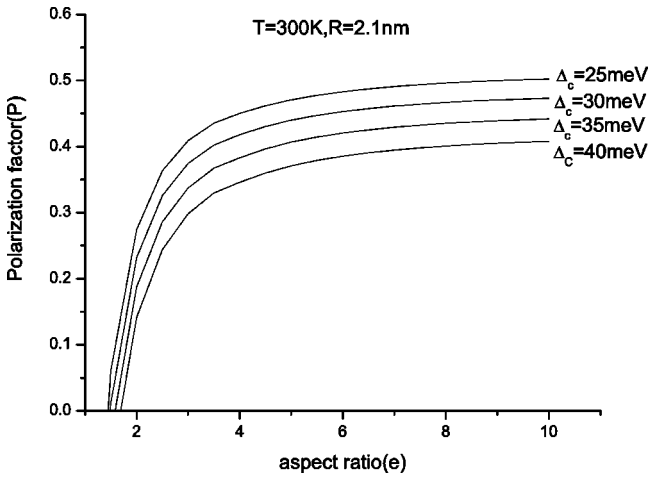

FIG. 5. P as a function of e in the case of $\Delta_c = 40$ meV, 35 meV, 30 meV, and 25 meV; all other parameters are the same as in Fig. 4.

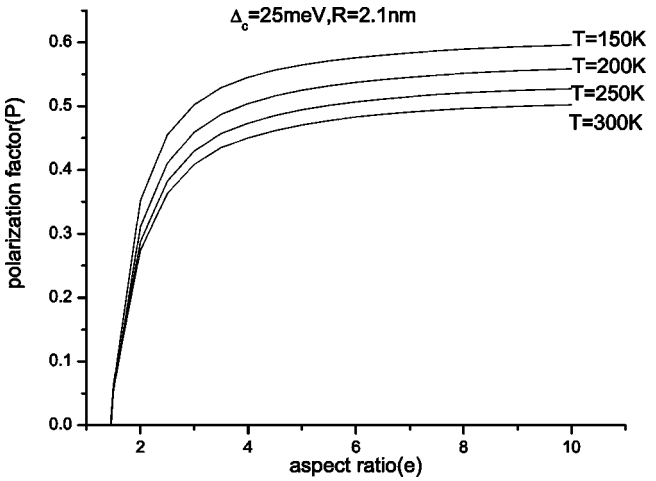

FIG. 6. P as a function of e in the case of $T = 150$ K, 200 K, 250 K, and 300 K; all other parameters are the same as in Fig. 4.

1. Effect of the crystal field splitting energy Δ_c

We have used $\Delta_c = 25$ meV (Ref. 13) (Table I) in the above calculation. Fig. 5 shows P as a function of e for $\Delta_c = 40$ meV,35 meV,30 meV, and 25 meV; we keep all other parameters unchanged. From Fig. 5 we see that the polarization factors for $\Delta_c = 40$ meV are smaller than those for $\Delta_c = 25$ meV, and the saturation value is about 0.4. For larger Δ_c, the S_z state, which is connected to the Z basic state of the valence band top, becomes higher relative to the ground state (P_x) connected to the X and Y basic states. The S_z component mixed into the ground, second, and third states decreases, resulting in a decrease in the contribution of these states to the z polarization. In Table II the contributions of the ground, 2-3, and 4-6 states of $J_z = 1/2$, and the ground state of $J_z = 3/2$ to the optical transitions of z and x polarizations are listed in the first, second, third, and fourth rows, respectively. The first column is for the normal case, and the second column is for the case of $\Delta_c = 40$ meV. Comparing the first and second columns we see that the contribution from ground state of $J_z = 1/2$ decreases by one-half. The contribution of the 4-6 states is very small so that it can be neglected.

2. Effect of temperature

Figure 6 shows P as a function of e for $T = 150$ K, 200 K, 250 K, and 300 K; all other parameters are the same as in Fig. 4. From Fig. 6 we see that the polarization factors increase compared to Fig. 4, and the saturation value for $T = 150$ K is about 0.6 compared to 0.5. Because of the Boltzmann distribution the contribution from the ground state of $J_z = 3/2$ (S_x) to the x polarization decreases largely, as shown in the third column of Table II. Though the contribution to the z polarization also decreases, the total effect is that the P increases.

3. Effect of transverse radius R

Figure 7 shows P as a function of e for $R = 2.1$ nm, 1.9 nm, 1.7 nm, and 1.5 nm; all other parameters are kept unchanged. From Fig. 7 we see that the polarization factors increase compared to those in Fig. 4, and the saturation value is 0.68 for $R = 1.5$ nm compared to 0.5 for $R = 2.1$ nm. Because the spacing of energy levels is $\sim 1/R^2$, for smaller R the spacing is larger, and the Boltzmann factor is smaller for high excited states, especially the ground state of $J_z = 3/2$ (S_x). The effect is similar to that of lowering the temperature, as shown in the fourth column in Table II.

D. Band gap

The band gap is another very important character for the optical properties of semiconductors. In our model, the boundary is too sharp compared with the actual case since

TABLE II. Contributions of the first, 2-3, and 4-6 states of $J_z = 1/2$ and the ground state of $J_z = 3/2$ to the transition strength I_z and I_x for four cases illustrated in the text.

$e = 4$	I_z				I_x			
Case	Normal	$\Delta_c = 40$ meV	$T = 150$ K	$R = 1.5$ nm	Normal	$\Delta_c = 40$ meV	$T = 150$ K	$R = 1.5$ nm
1/2, first	0.1500	0.0862	0.1500	0.2010	0.0342	0.0219	0.0342	0.0353
1/2, 2-3	0.2876	0.2741	0.1753	0.2815	0.0561	0.0589	0.0343	0.0405
1/2, 4-6	0.0010	0.0014	0.0001	0.0001	0.0001	0.0002	0.0000	0.0000
3/2, first					0.0759	0.0948	0.0273	0.0234
Sum	0.4385	0.3617	0.3254	0.4826	0.1663	0.1758	0.0958	0.0992
P	0.4501	0.3459	0.5451	0.6590				

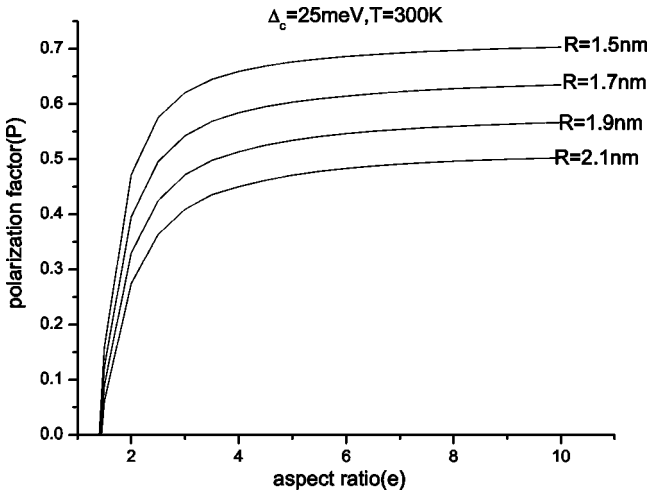

FIG. 7. P as a function of e in the case of $R=1.5$ nm, 1.7 nm, 1.9 nm, and 2.1 nm; all other parameters are the same as in Fig. 4.

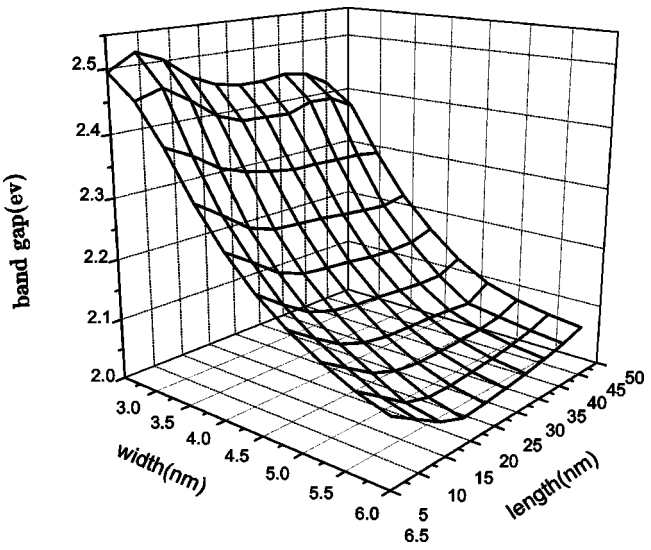

FIG. 8. Band gap of CdSe quantum rods vs length and width.

we assume that the electron and hole are in an infinitely deep well; we have not considered the exciton effect at the same time, so we just give a draft of how the length and width affect the band gap. There are two parameters that determine the width and length of the rod: the diameter and the aspect ratio. We give the draft in Fig. 8 by tuning these two parameters. From this figure, we see that the confinement in width has a much stronger effect than that in length on the gap.[14]

IV. CONCLUSIONS

The Hamiltonian of the wurtzite structure quantum rods with an ellipsoidal boundary is given after a coordinate transformation. The energies and wave functions are obtained with the same method we used on spherical dots. We tuned the aspect ratio of the rods, and found transition possibilities of z and x polarizations for transitions to the $J_z=1/2$ and $J_x=3/2$ hole states and the energies the two groups of hole states as functions of e. Both the transition matrix element and the Boltzmann distribution contribute to the emission properties of the quantum rods. With an overall consideration of these factors we explained why the polarization factor increases with increasing e and approaches a saturation value, which tallies quite well with the result reported by experiment. As e increases, more and more S_z states are mixed into the ground, second, and third states of $J_z=1/2$, resulting in an increase in the emission of z polarization I_z. It is just the linear terms of the momentum operator in the hole Hamiltonian that cause the mixing of S and P states in the hole ground state. The effects of the crystal field splitting energy, the temperature, and the transverse radius to the polarization are also considered. We also calculated the band gap variation with the size and shape of the quantum rods and gave a discussion of these results.

ACKNOWLEDGMENTS

This work is supported by the National Natural Science Foundation of China, the special funds for Major State Basic Research Project No. G001CB3095 of China, and a project of the Chinese Academy of Sciences: Nanometer Science and Technology.

[1] A.P. Alivisatos, Science **271**, 933 (1996).
[2] L.E. Brus, Appl. Phys. A: Solids Surf. **53**, 465 (1991).
[3] L. Manna, E.C. Scher, and A.P. Alivisatos, J. Am. Chem. Soc. **122**, 12700 (2000).
[4] A.P. Alivisatos, J. Phys. Chem. **100**, 13226 (1996).
[5] J.T. Hu, L.S. Li, W.D. Yang, L. Manna, L.W. Wang, and A.P. Alivisatos, Science **292**, 2060 (2001).
[6] M. Bruchez Jr., M. Moronne, P. Gin, S. Weiss, and S.P. Alivisatos, Science **281**, 2013 (1998).
[7] W.C.W. Chan and S. Nie, Science **281**, 2016 (1998).
[8] V.l. Klimov *et al.*, Science **290**, 314 (2000).
[9] J.B. Xia and J.B. Li, Phys. Rev. B **60**, 11 540 (1999).
[10] J.B. Xia, Phys. Rev. B **40**, 8500 (1989).
[11] J.B. Xia, J. Lumin. **70**, 120 (1996).
[12] A.R. Edmonds, *Angular Momentum in Quantum Mechanics* (Princeton University Press, Princeton, NJ, 1957) p. 68.
[13] Al.L. Efros, Phys. Rev. B **46**, 7448 (1992); Al.L. Efros, M. Rosen, M. Kuno, M. Nirmal, D.J. Norris, and M. Bawendi, *ibid.* **54**, 4843 (1996).
[14] L.S. Li, J.T. Hu, W.D. Yang, and A.P. Alivisatos, Nano Lett. **1**, 349 (2001).